LANGMUIR Article
Cite This: Langmuir 2019, 35, 15979−15984
pubs.acs.org/Langmuir

Deciphering How the Viscoelastic Properties of Mussel-Inspired Metal-Coordinate Transiently Cross-Linked Gels Dictate Their Tack Behavior

Erica Lai,[†] Bavand Keshavarz,[‡] and Niels Holten-Andersen*,[†]

[†]Department of Materials Science and Engineering, [‡]Department of Mechanical Engineering, Massachusetts Institute of Technology Cambridge, Massachusetts 02139, United States

Supporting Information

ABSTRACT: In recent years, researchers have incorporated mussel-inspired metal-coordinate cross-links into various types of gels to improve their mechanical properties, particularly toughness and self-healing. However, not much is understood about how the linear mechanical properties of these gels dictate their tack properties. In this study, we use shear rheology and tack tests to explore correlations between linear viscoelastic properties (i.e., plateau modulus, G_p, and characteristic relaxation time, τ_c) and tack behavior (i.e., peak stress, σ_{max}, and energy dissipation per volume, EDV) of transiently cross-linked hydrogels comprised of histidine-functionalized 4-arm PEG coordinated with Ni^{2+}. By using the Ni^{2+}-histidine ratio and polymer wt % of the transient networks to control their viscoelastic properties, we demonstrate a strong dependence of σ_{max} on G_p and τ_c. The observed correlation between network dynamics and mechanics under tensile load is in good quantitative agreement with a theoretical framework for σ_{max}, which includes the linear viscoelastic properties as parameters. EDV is also influenced by G_p and τ_c, and the EDV after reaching σ_{max} is additionally dependent on the polymer wt %. These findings are consistent with previously proposed molecular mechanics of reversible His_xNi^{2+} cross-links and provide us with new insights into the correlations between bulk mechanics and adhesive dynamics of gels with transient metal-coordinate cross-links.

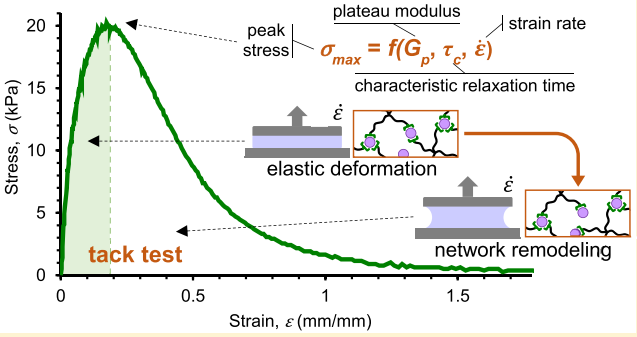

INTRODUCTION

Researchers seeking to design bioinspired adhesives for underwater or medical device applications have increasingly drawn inspiration from proteins within the mussel byssal threads.[1−3] In particular, focus has been on using modified amino acid ligands like 3,4-dihydroxyphenylalanine (Dopa), which is known to play an important role in surface adhesion and bulk cohesion within the mussel adhesive plaque (please see Figure 1a for a general schematic). Dopa contributes strongly to interfacial adhesion via bidentate coordination bonds, hydrogen bonds, and other noncovalent interactions. Within the mussel adhesive plaque, diDopa covalent cross-links and dynamic metal−ligand coordination cross-links jointly contribute to the formation of a strong and highly dissipative material.[4−6] It has been well established that the incorporation of mussel-inspired metal coordination cross-links into covalently cross-linked hydrogels can improve their bulk mechanical properties, particularly toughness and self-healing.[7,8] However, it remains unclear how metal-coordinate-based cross-link mechanisms affect the adhesive properties of a hydrogel.

Significant research efforts have been dedicated to understanding how the viscoelastic properties of reversibly cross-linked hydrogels can be controlled with mussel-inspired metal−ligand coordination chemistry. Specifically, the role of metal-coordinate cross-link dynamics in controlling gel mechanics in the linear mechanical regime has been extensively studied through the tuning of multiple physical-chemical parameters,[9−15] particularly in gels composed of four-arm polyethylene glycol (4PEG) end-functionalized with histidine (His).[7,12,14,15] Histidine is an amino acid also found within the mussel byssal thread, primarily in the thread core, which can coordinate with divalent transition metals like Ni^{2+} to form reversible His_xNi^{2+} complex cross-links (please see Figure 1b).

Using the metal−ligand ratio to control the concentration of His_xNi^{2+} complexes with different functionalities present within a gel (i.e., His_3Ni^{2+} and His_2Ni^{2+}, or tris- and bis-coordination complexes, respectively), the impact on plateau modulus (G_p), and characteristic relaxation time (τ_c) was determined.[14]

Through spatiotemporal hierarchical coordination, Dopa and histidine coordination complexes together are hypothe-

Special Issue: Intermolecular Forces and Interfacial Science

Received: September 3, 2019
Revised: October 21, 2019
Published: October 21, 2019

Downloaded via MASSACHUSETTS INST OF TECHNOLOGY on December 23, 2019 at 21:15:51 (UTC).
See https://pubs.acs.org/sharingguidelines for options on how to legitimately share published articles.

 © 2019 American Chemical Society
DOI: 10.1021/acs.langmuir.9b02772
Langmuir 2019, 35, 15979−15984

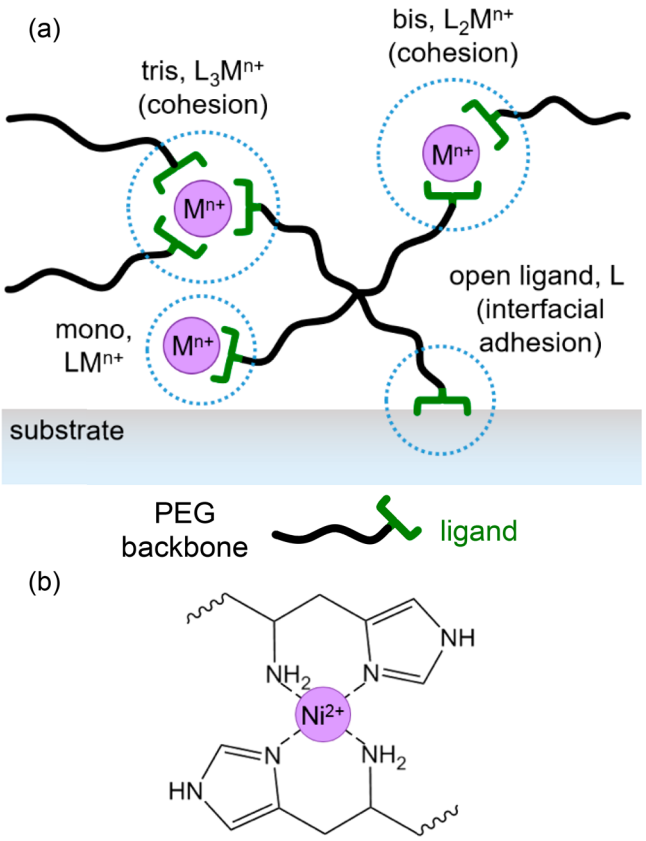

Figure 1. (a) Schematic of L_xM^{n+} complexes in a 4PEG-ligand (L) + metal ion (M^{n+}) transient hydrogel and their proposed contributions to gel cohesion and interfacial adhesion. (b) Chemical structure of a His_2Ni^{2+} complex.

sized to contribute to the energy dissipative and self-healing behavior of mussel adhesive threads.[7,16−19] However, in these initial investigations of the adhesive properties of mussel-inspired metal-coordinate cross-linked hydrogels, we chose to focus exclusively on histidine as the coordinating ligand because of its insensitivity to auto-oxidation. Accordingly, the adhesive tack properties of fully transient (i.e., dynamically cross-linked) hydrogels consisting of 10 kDa 4PEG-His coordinated with Ni^{2+} were assessed for the first time. It is important to note that this fully transient model gel system is technically a viscoelastic fluid even if it has gel-like behavior on the time scales studied. By controlling the bulk gel network density and dynamics via the Ni^{2+}-His ratio (0.25−0.5) and the polymer weight percent (5 and 10 wt %), we were able to quantify the dependence of nonlinear properties, such as peak stress (σ_{max}) and energy dissipation per volume (EDV) extracted from tack tests performed at different constant strain rates ($\dot{\varepsilon}$), on the linear viscoelastic properties G_p and τ_c. We are able to account for the experimental measurements of σ_{max} with a theoretical framework which incorporates G_p and τ_c. The amount of energy dissipated by the gel networks before and after peak stress is as expected also influenced by G_p and τ_c, even though it is not captured by our theoretical model. Furthermore, the EDV after reaching σ_{max} appears to display an additional dependence on network density, plausibly due to an effect of network remodeling dynamics during deformation. Thus, our experimental findings are consistent with previously proposed molecular mechanics of the dynamic His_xNi^{2+} cross-links. By deciphering the contributions of metal-coordinate cross-linking to the tack properties of physical hydrogels, this study provides insights into how metal coordinate dynamic cross-linking can be used to potentially tune the adhesive properties of future hydrogel materials.

■ EXPERIMENTAL SECTION

Synthesis of 4PEG-His. The full synthesis procedure for 10 kDa four-arm histidine-modified polyethylene glycol (4PEG-His) can be found in Grindy et al. but is summarized here.[14] First, 1−3 g of four-arm PEG-NH_2·HCl (0.25 equiv PEG, 1.0 equiv -NH_2 groups) (10 kDa, from JenKem U.S.A.) is mixed with Boc-His(Trt)-OH (1.5 equiv) and BOP reagent (1.5 equiv) and is dissolved in 15 mL of dichloromethane (DCM). *N,N*-Diisopropylethylamine (DIPEA) (535 equiv) is added, and the reaction proceeds for 2 h under N_2 at room temperature. Then, the product is purified by precipitation in diethyl ether one time, methanol at −20 °C one time, and diethyl ether once again, and then the product is vacuum-dried. To remove the protecting groups from the histidines, a cleavage solution of 95 mL of trifluoroacetic acid (TFA), 2.5 mL of triisopropylsilane, and 2.5 mL of water is added and the reaction proceeds for 2 h at room temperature. The solvent is removed under reduced pressure, and the product is then purified by redissolution in methanol, precipitation in ether three times, and vacuum-drying.

Synthesis of 4PEG-His + Ni^{2+} Hydrogel Samples. The appropriate volume of 0.1 M phosphate buffer solution, pH 7.4, is added to the polymer in a centrifuge tube, and the mixture is vortexed until the solution is well-mixed. This 4PEG-His solution is then pipetted onto a piece of Parafilm and combined with a small volume of 0.2 M solution of nickel(II) chloride hexahydrate ($NiCl_2·6H_2O$), resulting in a 10 wt % gel with the desired stoichiometric ratio of Ni^{2+} to histidine; in this study, the ratio range was 0.25−0.5. The gel is kneaded using the Parafilm, until it is homogeneous, and stored in a 1.7 mL centrifuge tube until testing to prevent dehydration. For a 5 wt % gel, more phosphate buffer is added to dilute the 10 wt % gel.

Small Angle Oscillatory Shear (SAOS). Shear rheology is performed on an Anton Paar MCR 302 rheometer with a 10 mm-diameter parallel plate (PP10), i.e., R_0 = 5 mm, a glass substrate at room temperature (∼22 °C), and a gap of 0.300 mm, scanning a frequency range of 100 to 0.1 rad/s with a strain amplitude of 0.1%. A solvent trap is used during the test to minimize dehydration.

Tack Tests. All tack tests are performed on an Anton Paar MCR 302 rheometer at room temperature using PP10 as a probe. The bottom substrate is a glass slide that sits atop a support containing a 45° mirror allowing bottom-up video recording of the gel sample during experiments. A fresh gel sample is used for each individual run. During a test, the probe is brought into contact with the gel sample at 50 μm/s. The gel is trimmed to the dimensions of the probe when the gap size is 0.325 mm. Once the gel is compressed to an initial thickness, h_0, of 0.300 mm, it is allowed to relax to zero normal force. While the exact contact time was not precisely controlled, it was ensured that the contact time was at least ten times longer than the characteristic relaxation time scale (i.e., at least 30 s), and the assumption is that the gel has reached chemical equilibrium with the probe surface. At that point, the probe is retracted at a constant strain rate ($\dot{\varepsilon}$), which is obtained by creating an exponential moving profile on the rheometer (please see Figure 2a). This generates a force−displacement curve, which is then converted to an engineering stress−strain curve up to 178% engineering strain (to 0.834 mm) to determine peak stress, σ_{max}, and the energy dissipation per volume, EDV (in units of J/m^3). A distinction is made between the EDV before σ_{max} is reached, "pre-peak EDV", and the EDV after σ_{max} is reached, "post-peak EDV". A schematic representation of these parameters is presented in Figure 2b.

Theoretical Prediction for the Temporal Evolution of the Tack Force. We use the following theoretical framework to account for the evolution of tack force over time. During a tack test, the gap between the probe and substrate remains much smaller than the plate radius, i.e., $h(t) \ll R_0$. Thus, for noncavitation cases, we can assume that the flow in the thin gap is dominated by viscous effects and the

DOI: 10.1021/acs.langmuir.9b02772
Langmuir 2019, 35, 15979−15984

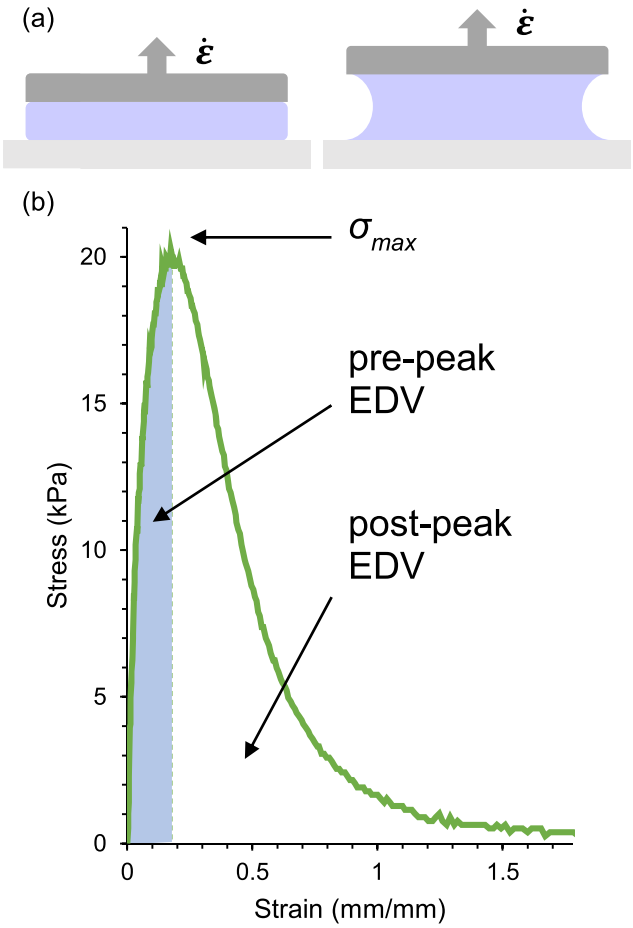

Figure 2. (a) Schematic of a constant strain rate tack test (dimensions are not to scale). (b) Representative stress−strain tack test curve defining peak stress (σ_{max}) and pre-peak and post-peak energy dissipation per volume (EDV).

pressure gradient under the plate is mainly balanced by the gradient of viscous stresses (similar to squeeze flow or Stefan's flow).[20] We can also assume that the apparent adhesion force is due to the suction pressure that is generated through the action of viscous stresses in the flow. Spiegelberg et al. studied this flow for viscous Newtonian fluids and found an approximate solution for the flow kinematics in this problem.[21] It has been shown that the described Newtonian kinematics is fairly accurate even for viscoelastic liquids.[22] The approximate kinematics can be coupled with linear constitutive equations, such as the Maxwell model (one spring and one dashpot in series), which leads to a theoretical prediction for the temporal evolution of the adhesion force, $F(t)$, in eq 1

$$\frac{F(t)}{G_p \pi {R_0}^2} = \frac{\sigma(t)}{G_p} = 3\left(\frac{R_0}{h_0}\right)^2 \frac{Wi}{1-2Wi}\left[\exp\left(-2Wi\frac{t}{\tau_c}\right) - \exp\left(-\frac{t}{\tau_c}\right)\right]\left[\exp\left(-2Wi\frac{t}{3\tau_c}\right) - \frac{1}{2}\exp\left(-3Wi\frac{t}{\tau_c}\right)\right] \quad (1)$$

where the geometrical parameters R_0 and h_0 represent the plate radius and the initial gap height, and Wi is the Weissenberg number ($Wi \equiv \tau_c\dot{\varepsilon}$). This relationship shows that the maximum adhesion force is set by a combination of the linear rheological properties, geometrical factors, and Wi. The maximum of this expression can be easily calculated at different Wi, and the suggested model can be compared to experimental measurements. A more detailed derivation is provided in the Supporting Information (S1).

RESULTS AND DISCUSSION

Linear Viscoelastic Properties (G_p and τ_c) of Transiently Cross-linked 4PEG-His + Ni^{2+} Hydrogels. As introduced above, the model system consists of 10 kDa 4PEG-His polymers forming strong yet reversible bonds with Ni^{2+} to create a transiently cross-linked viscoelastic hydrogel. To determine how their linear viscoelastic properties affect tack behavior, we first performed oscillatory frequency sweeps in shear on all hydrogel samples. Because the hydrogels exhibited single-mode Maxwellian behavior, a single G_p and τ_c was obtained from each frequency sweep when fitted, as shown in Figure S1. The trends in the average G_p and τ_c with respect to the Ni^{2+}-His ratio match those previously reported in Grindy et al. (see Figure S2),[14] wherein the value of G_p was demonstrated to scale with the predicted amount of elastically active chains in the gel network, as described by eq 2

$$G_p^{\text{predicted}} \propto \frac{[\text{His}_2\text{Ni}^{2+}] + 3[\text{His}_3\text{Ni}^{2+}]}{[\text{His}]_{\text{total}}} \quad (2)$$

The τ_c trend also matches that found in Grindy et al., even if the polymer molecular weight and gel wt % studied were different.[14,23]

Qualitative Categorization of the Tack Tests via Visual Documentation. On the basis of video recorded during the tack test, each tested sample was qualitatively placed into one of three categories: (a) no cavitation, no rupture, (b) no cavitation, rupture, and (c) cavitation. Representative cross-sectional sample snapshots for each category can be found in Figure S3; corresponding stress−strain curve shapes are included as well. In the cases where no cavitation or rupture is detected, the sample stays well-adhered at the probe and substrate interfaces and is drawn into a single central fibril. "Rupture" is defined as a rip that forms when the pressure inside the elongating fibril suddenly equalizes with its environment, but the sample does not debond from the substrate or the probe. The transition from "no rupture" to "rupture" occurs when the strain rate is increased and/or the gel composition results in a stiffer, slower-relaxing sample and is represented in the shape of the stress−strain curve by a sharp decrease in stress. "Cavitation" is defined as the formation and growth of air bubbles from the interface of the fixed glass substrate and potentially into the bulk gel due to negative hydrostatic stress created in this sample geometry (i.e., a radius much larger than its thickness).[24] The presence of cavitation is independent of the presence of rupture, but cavitation tends to occur at higher strain rates and in stiffer, slower-relaxing gel samples; if rupture does occur, it usually happens at lower strains when cavitation also exists.

Unlike in traditional pressure sensitive adhesives, which typically contain much longer-lived cross-links, no stress plateau corresponding to fibrillation is observed after the peak stress.[25] Instead, we observe an exponential decay after the peak stress (or after a rupture event occurs). We attribute this to the fully transient nature and narrow distribution of dynamic cross-link time scales of the metal-coordinate model system; however, more investigation is required to confirm this hypothesis.

Relationship between Peak Stress (σ_{max}) and Linear Viscoelastic Properties. To determine how the tack

DOI: 10.1021/acs.langmuir.9b02772
Langmuir 2019, 35, 15979−15984

properties of a hydrogel may be influenced by its linear rheological behavior, i.e., G_p and τ_c, we first investigated how σ_{max} changes with $\dot{\varepsilon}$ (0.1−1.6 1/s) and gel composition (Figure 3). The *Y*-axis error bars indicate the lowest and highest values recorded for a given data point after averaging the results.

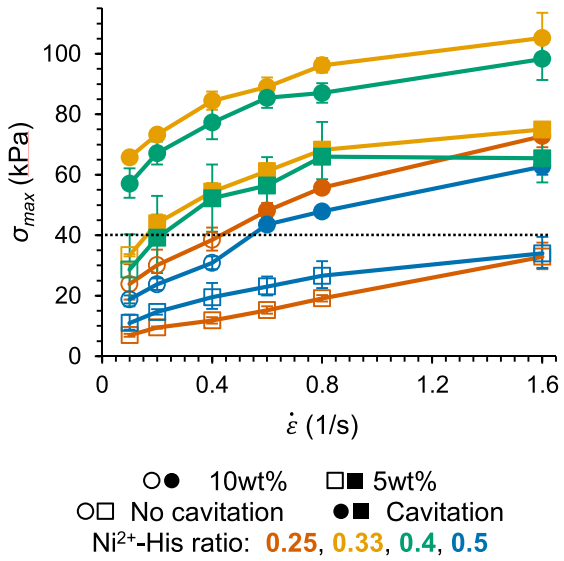

Figure 3. Peak stresses (σ_{max}) achieved by 4PEG-His + Ni^{2+} gels during tack tests at a given strain rate ($\dot{\varepsilon}$). A composition-independent threshold was empirically found at around 40 kDa (indicated by a dashed line), below which no gel sample cavitation occurred.

We noticed three trends that correspond well to those found in traditional pressure sensitive adhesives (PSAs),[25] even though our model system is fully transient. First, with increasing $\dot{\varepsilon}$ in the range studied, σ_{max} increases toward a plateau. Second, for each Ni^{2+}-His ratio, 10 wt % gels reach higher σ_{max} values than their 5 wt % counterparts. And third, within a given wt %, a gel with a higher G_p reaches higher σ_{max} values. Like in PSAs, σ_{max} increases with strain rate due to viscoelastic losses and correlates well with the storage modulus (G'), which at the strain rates tested is effectively G_p.[25]

To determine the effect of the linear mechanical properties of G_p and τ_c on the value of σ_{max}, dimensionless variables are created; $\dot{\varepsilon}$ is multiplied by τ_c to generate the Weissenberg number, *Wi*, while σ_{max} is divided by G_p (please see Figure S4 for a full data plot of each individual gel sample accordingly). Generally speaking, σ_{max} is dictated by the competition between elastic chain deformation and plasticity introduced by dissociating cross-links. However, the onset of cavitation reduces σ_{max} and the propagation of the cavities tends to induce inconsistent catastrophic rupture and/or failure. Going forward, we therefore only focus on gel samples that did not undergo cavitation, which could be experimentally determined via an empirical cavitation threshold of approximately 40 kPa (i.e., the dotted line in Figure 3). In Figure 4, we plot the samples that did not undergo cavitation alongside the linear mechanical theoretical model (as derived from eq 1). The experimental data points are found to match the model prediction well, which strongly indicates that the gel network density, as quantified by G_p, and the gel network dynamics, as quantified by τ_c, indeed determine σ_{max}.

The gel samples that exhibited rupture are observed to fall slightly below the theoretical prediction, which may be caused

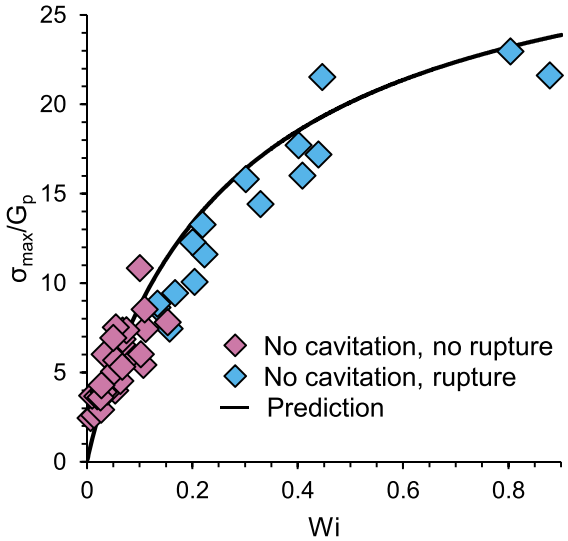

Figure 4. σ_{max}/G_p vs *Wi* for gel samples with no cavitation (symbols) compared to the theoretical prediction derived from eq 1 (line). The color of the symbol also indicates whether the corresponding gel sample experienced rupture (blue) or not (pink).

by the expansion of initially optically invisible air bubble defects allowing for premature rupture to occur thereby slightly reducing σ_{max}.

Relationship between Energy Dissipation and Linear Viscoelastic Properties. Because our model material tends to draw into a single fibril and undergo large extension ratios rather than debond at the interface, adhesion energy (J/m^2) is not a relevant measure for characterizing its tack properties.[26] Instead, we defined EDV with units of J/m^3 by accounting for the initial thickness of the sample as well. Like the σ_{max} analyses, EDV comparisons were only done with gels that did not undergo cavitation. Like σ_{max} vs $\dot{\varepsilon}$, EDV, pre-peak EDV, and post-peak EDV have similar trends regarding $\dot{\varepsilon}$, wt %, and G_p; EDV increases with $\dot{\varepsilon}$, 10 wt % gels have higher EDVs than 5 wt % gels, and a gel with a higher G_p has a higher EDV. These trends, which can be observed in Figure S5a−c, are due to an increase in viscoelastic losses as $\dot{\varepsilon}$ increases and are consistent with previous studies.[25] When the axes are made dimensionless, i.e., EDV/G_p vs *Wi* (Figure S 5d), more insightful trends can be observed, especially when split into the pre-peak and post-peak EDV/G_p vs *Wi* graphs shown in Figure 5.

The results suggest that in addition to being influenced by G_p and τ_c, post-peak EDV is also dependent on wt %. These findings are consistent with the proposed molecular mechanics of reversible cross-links, in the following way. Prior to reaching σ_{max}, the gel predominantly undergoes elastic deformation under the applied load; the ligands in the coordination cross-links have not yet detached and relaxed, and so the elastically active chains (whose fraction is dictated by the metal−ligand ratio) determine both the pre-peak EDV and G_p. Therefore, pre-peak EDV/G_p should not have an additional dependence on gel composition. However, after reaching σ_{max}, remodeling, i.e., the ligand detachment and/or exchange between complexes, results in a reduction of elastically active chains. Since the probability for successful ligand exchange to occur decreases with increased polymer wt %, possibly due to hindered molecular motion as a ligand tries to find a different complex to join, the observed increase post-peak EDV/G_p

DOI: 10.1021/acs.langmuir.9b02772
Langmuir 2019, 35, 15979−15984

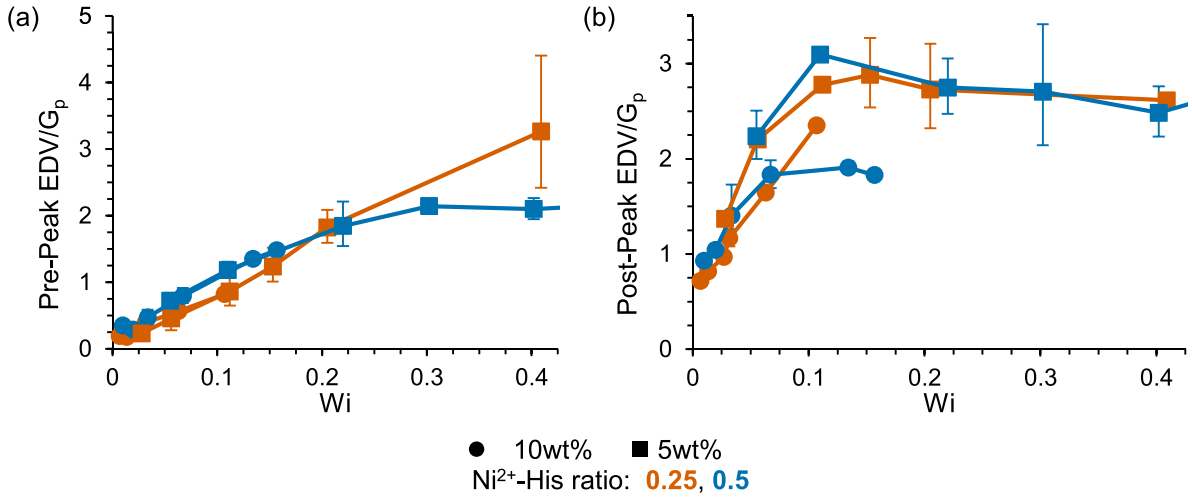

Figure 5. EDV/G_p, (a) pre-peak and (b) post-peak, vs *Wi* for noncavitation cases of tack tests on 4PEG-His gels. The results for the Ni^{2+}-His ratios of 0.33 and 0.4 are not plotted because there were not enough noncavitation cases to analyze. The alignment of the pre-peak EDV data indicates that like for σ_{max}, pre-peak EDV is predominantly influenced by G_p and τ_c. Post-peak EDV, on the other hand, has an additional dependence on polymer wt %.

makes sense.[27−30] The effect of wt % on cross-link density is encapsulated in G_p, but its effect on network remodeling in the post-peak region of the stress−strain curve is not, hence the additional dependence.

■ CONCLUSIONS

In this study, we demonstrated how strongly the tack parameters of peak stress (σ_{max}) and energy dissipation per volume (EDV) correlated with the linear rheological properties of plateau modulus (G_p) and characteristic relaxation time (τ_c) for 4PEG-His + Ni^{2+} gels during tack tests with no cavitation. For σ_{max}, a theoretical model was developed that had the temporal evolution of the tack force dependent on G_p, τ_c, the Weissenberg number (*Wi*), and geometrical factors; this model was then compared to experimental data to further demonstrate this relationship. For energy dissipation per volume, in addition to the dependency of EDV on linear rheological properties, the polymer wt % affects the EDV after the peak stress is reached because network density affects the ability of the gel to remodel at higher strains. This study demonstrates that when tensile tests cannot be performed, tack tests can provide comparable information. With mussel-inspired metal coordinate cross-links providing methods to tailor the relaxation spectrum of a viscoelastic hydrogel, these findings can inform the design of better adaptable adhesives.

While this study already provides pertinent information regarding the possible use of metal coordination in future hydrogel adhesives, further investigation is needed in two areas. First, since adhesion is a balance of cohesive and interfacial strength, attention must be paid to behavior at the gel-substrate interface; this can be done by performing tests on multiple substrates with different surface energies or roughness or by including a primer layer. Interfacial physics and mechanics on the mesoscopic length scales should also be studied. Second, knowledge obtained from the Ni^{2+}-His transient gel model system can be applied to a Fe^{3+}-Dopa cross-linked gel in an effort to decouple the combined effects of coordinate and covalent bonds within this hybrid system; the mix of covalent and metal-coordinate bonds better matches what is likely present in a mussel's adhesive plaque. The performance of tack tests on Fe^{3+}-Dopa gels and the connection of tack parameters to linear rheological properties would also provide us with an understanding of the adhesive dynamics of these gels and thus inform the design of underwater or medical adhesives.

■ ASSOCIATED CONTENT

Supporting Information

The Supporting Information is available free of charge on the ACS Publications website at DOI: 10.1021/acs.langmuir.9b02772.

> Full derivation of the theoretical prediction for the temporal evolution of the tack force, a representative frequency sweep for one of the 4PEG-His + Ni^{2+} hydrogels studied, average G_p and τ_c for the gels, a schematic depicting the three qualitative categories of sample behavior, σ_{max}/G_p vs *Wi* with the cavitation cases included, EDV vs strain rate and total EDV/G_p vs *Wi* graphs for noncavitation cases of tack tests on the gels (PDF)

■ AUTHOR INFORMATION

Corresponding Author

*E-mail: holten@mit.edu.

ORCID

Bavand Keshavarz: 0000-0002-1988-8500

Niels Holten-Andersen: 0000-0002-5318-9674

Notes

The authors declare no competing financial interest.

■ ACKNOWLEDGMENTS

This work is financially supported in part by the Office of Naval Research (ONR) under the Young Investigators Program Grant ONR.N00014-15-1-2763 and the MRSEC Program of the National Science Foundation under Award DMR-1419807. In addition, E.L.'s work is supported in part by the Anne M. Mayes Fellowship through the Department of Materials Science and Engineering at MIT as well as by the National Science Foundation via the Graduate Research

DOI: 10.1021/acs.langmuir.9b02772
Langmuir 2019, 35, 15979−15984

Fellowship Program under Grant No. 2388357. The authors would like to thank their colleagues in the Laboratory for Bio-Inspired Interfaces, their collaborators Daniel Darby and Dr. Jonathan Pham (University of Kentucky), and members of the adhesion community for their insights and support.

■ REFERENCES

(1) Lee, B. P.; Messersmith, P. B.; Israelachvili, J. N.; Waite, J. H. Mussel-Inspired Adhesives and Coatings. *Annu. Rev. Mater. Res.* **2011**, *41*, 99−132.

(2) Brubaker, C. E.; Messersmith, P. B. The Present and Future of Biologically-Inspired Adhesive Interfaces and Materials. *Langmuir* **2012**, *28*, 2200−2205.

(3) Cui, M.; Ren, S.; Wei, S.; Sun, C.; Zhong, C. Natural and Bio-Inspired Underwater Adhesives: Current Progress and New Perspectives. *APL Mater.* **2017**, *5*, 116102.

(4) Lee, H.; Scherer, N. F.; Messersmith, P. B. Single-Molecule Mechanics of Mussel Adhesion. *Proc. Natl. Acad. Sci. U. S. A.* **2006**, *103* (35), 12999−13003.

(5) Waite, J. H. Mussel Adhesion − Essential Footwork. *J. Exp. Biol.* **2017**, *220* (4), 517−530.

(6) Ahn, B. K. Perspectives on Mussel-Inspired Wet Adhesion. *J. Am. Chem. Soc.* **2017**, *139* (30), 10166−10171.

(7) Fullenkamp, D. E.; He, L.; Barrett, D. G.; Burghardt, W. R.; Messersmith, P. B. Mussel-Inspired Histidine-Based Transient Network Metal Coordination Hydrogels. *Macromolecules* **2013**, *46* (3), 1167−1174.

(8) Fullenkamp, D. E.; Barrett, D. G.; Miller, D. R.; Kurutz, J. W.; Messersmith, P. B. PH-Dependent Cross-Linking of Catechols through Oxidation via Fe 3+ and Potential Implications for Mussel Adhesion. *RSC Adv.* **2014**, *4* (48), 25127−25134.

(9) Holten-Andersen, N.; Harrington, M. J.; Birkedal, H.; Lee, B. P.; Messersmith, P. B.; Lee, K. Y. C.; Waite, J. H. PH-Induced Metal-Ligand Cross-Links Inspired by Mussel Yield Self-Healing Polymer Networks with near-Covalent Elastic Moduli. *Proc. Natl. Acad. Sci. U. S. A.* **2011**, *108* (7), 2651−2655.

(10) Barrett, D. G.; Fullenkamp, D. E.; He, L.; Holten-Andersen, N.; Lee, K. Y. C.; Messersmith, P. B. PH-Based Regulation of Hydrogel Mechanical Properties through Mussel-Inspired Chemistry and Processing. *Adv. Funct. Mater.* **2013**, *23* (9), 1111−1119.

(11) Kawamoto, K.; Grindy, S. C.; Liu, J.; Holten-Andersen, N.; Johnson, J. A. Dual Role for 1,2,4,5-Tetrazines in Polymer Networks: Combining Diels-Alder Reactions and Metal Coordination to Generate Functional Supramolecular Gels. *ACS Macro Lett.* **2015**, *4* (4), 458−461.

(12) Grindy, S. C.; Learsch, R.; Mozhdehi, D.; Cheng, J.; Barrett, D. G.; Guan, Z. B.; Messersmith, P. B.; Holten-Andersen, N. Control of Hierarchical Polymer Mechanics with Bioinspired Metal-Coordination Dynamics. *Nat. Mater.* **2015**, *14* (12), 1210−1216.

(13) Li, Q.; Barrett, D. G.; Messersmith, P. B.; Holten-Andersen, N. Controlling Hydrogel Mechanics via Bio-Inspired Polymer−Nanoparticle Bond Dynamics. *ACS Nano* **2016**, *10* (1), 1317−1324.

(14) Grindy, S. C.; Lenz, M.; Holten-Andersen, N. Engineering Elasticity and Relaxation Time in Metal-Coordinate Cross-Linked Hydrogels. *Macromolecules* **2016**, *49* (21), 8306−8312.

(15) Grindy, S. C.; Holten-Andersen, N. Bio-Inspired Metal-Coordinate Hydrogels with Programmable Viscoelastic Material Functions Controlled by Longwave UV Light. *Soft Matter* **2017**, *13* (22), 4057−4065.

(16) Vaccaro, E.; Waite, J. H. Yield and Post-Yield Behavior of Mussel Byssal Thread: A Self-Healing Biomolecular Material. *Biomacromolecules* **2001**, *2* (3), 906−911.

(17) Zhao, H.; Waite, J. H. Proteins in Load-Bearing Junctions: The Histidine-Rich Metal-Binding Protein of Mussel Byssus. *Biochemistry* **2006**, *45* (47), 14223−14231.

(18) Harrington, M. J.; Waite, J. H. Holdfast Heroics: Comparing the Molecular and Mechanical Properties of Mytilus Californianus Byssal Threads. *J. Exp. Biol.* **2007**, *210* (24), 4307−4318.

(19) Schmidt, S.; Reinecke, A.; Wojcik, F.; Pussak, D.; Hartmann, L.; Harrington, M. J. Metal-Mediated Molecular Self-Healing in Histidine-Rich Mussel Peptides. *Biomacromolecules* **2014**, *15* (5), 1644−1652.

(20) Stefan, J. Versuche Über Die Scheinbare Adhäsion. *Ann. Phys.* **1875**, *230* (2), 316−318.

(21) Spiegelberg, S. H.; Ables, D. C.; McKinley, G. H. The Role of End-Effects on Measurements of Extensional Viscosity in Filament Stretching Rheometers. *J. Non-Newtonian Fluid Mech.* **1996**, *64* (2−3), 229−267.

(22) Jaishankar, A. *The Linear and Nonlinear Rheology of Multiscale Complex Fluids*; Massachusetts Institute of Technology: 2014.

(23) Parada, G. A.; Zhao, X. Ideal Reversible Polymer Networks. *Soft Matter* **2018**, *14* (25), 5186−5196.

(24) Crosby, A. J.; Shull, K. R.; Lakrout, H.; Creton, C. Deformation and Failure Modes of Adhesively Bonded Elastic Layers. *J. Appl. Phys.* **2000**, *88* (5), 2956−2966.

(25) Lakrout, H.; Sergot, P.; Creton, C. Direct Observation of Cavitation and Fibrillation in a Probe Tack Experiment on Model Acrylic Pressure-Sensitive-Adhesives. *J. Adhes.* **1999**, *69* (3−4), 307−359.

(26) Zosel, A. Molecular Structure, Mechanical Behaviour and Adhesion Performance of Pressure Sensitive Adhesives. *Adhes Sealants Ind. Mag* **2001**, 193−203.

(27) Yount, W. C.; Loveless, D. M.; Craig, S. L. Small-Molecule Dynamics and Mechanisms Underlying the Macroscopic Mechanical Properties of Coordinatively Cross-Linked Polymer Networks. *J. Am. Chem. Soc.* **2005**, *127* (41), 14488−14496.

(28) Yount, W. C.; Loveless, D. M.; Craig, S. L. Strong Means Slow: Dynamic Contributions to the Bulk Mechanical Properties of Supramolecular Networks. *Angew. Chem., Int. Ed.* **2005**, *44* (18), 2746−2748.

(29) Mozhdehi, D.; Neal, J. A.; Grindy, S. C.; Cordeau, Y.; Ayala, S.; Holten-Andersen, N.; Guan, Z. Tuning Dynamic Mechanical Response in Metallopolymer Networks through Simultaneous Control of Structural and Temporal Properties of the Networks. *Macromolecules* **2016**, *49* (17), 6310−6321.

(30) Tang, S.; Olsen, B. D. Relaxation Processes in Supramolecular Metallogels Based on Histidine-Nickel Coordination Bonds. *Macromolecules* **2016**, *49* (23), 9163−9175.

DOI: 10.1021/acs.langmuir.9b02772
Langmuir 2019, 35, 15979−15984